Geophysical Research Letters

RESEARCH LETTER
10.1029/2019GL083989

Weak Near-Field Behavior of a Tsunami Earthquake: Toward Real-Time Identification for Local Warning

V.J. Sahakian[1], D. Melgar[1], and M. Muzli[2,3]

[1]Department of Earth Sciences, University of Oregon, Eugene, OR, USA, [2]Earth Observatory of Singapore, Nanyang Technological University, Singapore, [3]Agency for Meteorology, Climatology, and Geophysics, Jakarta, Indonesia

Key Points:
- Near-field seismic data show that tsunami earthquakes radiate energy inefficiently, producing low accelerations
- Near-field geodetic data indicate that these earthquakes produce displacements approximately equal to similarly sized events
- These data can be combined as a proxy radiated energy to moment ratio, to discriminate the events in real time for local tsunami warning

Supporting Information:
- Supporting Information S1

Correspondence to:
V. J. Sahakian,
vjs@uoregon.edu

Citation:
Sahakian, V. J., Melgar, D., & Muzli, M. (2019). Weak near-field behavior of a tsunami earthquake: Toward real-time identification for local warning. *Geophysical Research Letters*, *46*. https://doi.org/10.1029/2019GL083989

Received 3 JUN 2019
Accepted 8 AUG 2019
Accepted article online 13 AUG 2019

Abstract Tsunami earthquakes produce some of the most devastating tsunamis. These rare events have comparatively modest magnitudes but rupture the shallowest portion of a subduction zone megathrust with exceptionally large seafloor displacements. Previous teleseismic observations found that they radiate seismic waves weakly. They should therefore not be strongly felt in the near field, but to date no near-source seismic recordings of these events exist that confirm this. Here we analyze near-field records of a tsunami earthquake, the 2010 **M**7.7 Mentawai, Indonesia event, which show remarkably weak shaking. This is strong evidence that this earthquake does indeed have a weakly radiating or inefficient source process, in spite of its large slip. Finally, we find that, when combined with near-source Global Navigation Satellite System displacement recordings it is possible to correctly characterize tsunami earthquakes in real-time and to provide local tsunami warning which is currently out of reach today for monitoring agencies.

Plain Language Summary This study looked at seismometer and GPS data near a tsunami earthquake—a moderate-sized earthquake that produced a very large tsunami for its size. We found that the seismic data infers the earthquake is small, but the GPS data are more in line with the size that the earthquake actually is. This fits with our hypothesis that tsunami earthquakes happen in the really shallow Earth near the seafloor, and break soft rock—so they do not create strong shaking (which is why the seismic data think the earthquake is small), but they do still deform the nearby coastline (why the GPS think the earthquake is more normal). The fact that it breaks the seafloor is why it produces such a large tsunami. This means that we can use "near-field" seismic and GPS data together to discriminate events as a tsunami earthquake or not by the time they have ruptured, thus allowing us to issue local tsunami warnings for the earthquake—something current algorithms cannot do.

1. Introduction

According to conceptual models of the depth-varying properties of megathrust earthquakes (Lay et al., 2012), "tsunami earthquakes" rupture the shallow-most (<10–15 km) seismogenic region of a subduction zone (Domain A, Figure 1) with large fault slip to the seafloor. In contrast, the majority of similarly sized earthquakes rupture the plate interface at greater depth within Domains B and C. Domain A is characterized by very compliant (Bilek & Lay, 1999), fluid-rich rocks with predominantly velocity strengthening frictional properties (Faulkner et al., 2011) that rarely lead to coseismic rupture. When an earthquake does occur, rupture is very slow (~1.0–1.5 km/s; Ammon et al., 2006; Lay et al., 2011) due to a low rigidity, but this does not inhibit large slip. In fact, large slip is required in order to produce a given moment. Figure 1 shows a schematic of this megathrust domain structure, with examples of well-observed finite fault models from several recent earthquakes in the same magnitude range (Jara et al., 2018; Melgar et al., 2017; Nocquet et al., 2017; Yue et al., 2013; Yue et al., 2014), ~**M**7.6–7.8 (moment magnitude). Of these, only the 2010 Mentawai earthquake (Hill et al., 2012; Lay et al., 2011; Yue et al., 2014) is a "tsunami" earthquake. It slipped up to 20 m in the shallow megathrust and does not at all rupture Domains B or C. In contrast, other similarly sized events rupture the deeper domains, but with lower (~3 m) average slip.

Large shallow slip invariably leads to large displacements on the seafloor and very hazardous tsunamis. The 1992 **M**7.6 Nicaragua, 1994 **M**7.8 Java, 2006 **M**7.7 Java, and 2010 **M**7.8 Mentawai earthquakes are examples of such events, which respectively produced up to 10, 14, 21, and 17 m of near-field tsunami runup (Baptista et al., 1993; Fritz et al., 2007; Hill et al., 2012; Synolakis et al., 1995). For their runup, the magnitudes of these earthquakes are comparatively modest. Most megathrust events in this magnitude range produce only small

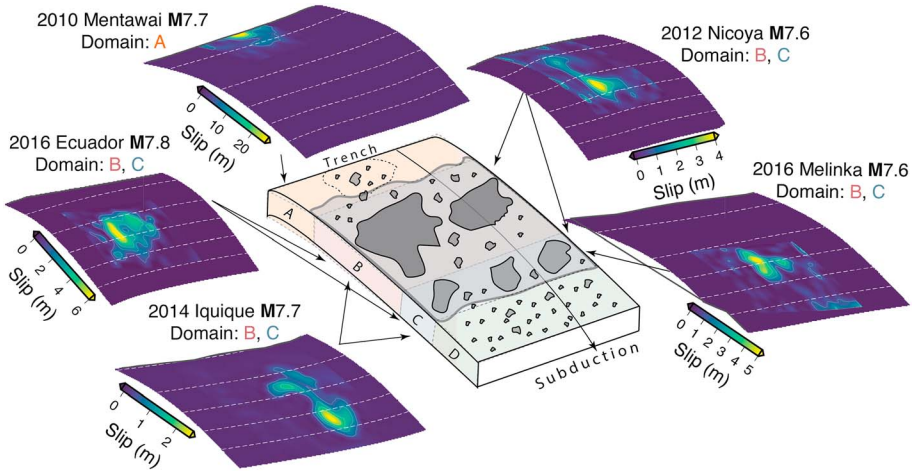

Figure 1. Schematic of megathrust rupture domains, with slip models from five representative earthquakes in the range 7.6 < **M** < 7.8. The center diagram is of a downgoing oceanic slab, modeled and demonstrates the paradigm of megathrust rupture domains (Lay et al., 2012). The trench is labeled, as well as an arrow indicating the direction of subduction. Each domain (A–D) is shaded a different color and shows unstable sliding regions as dark gray. The lighter gray region around Domains B and C shows the area where most megathrust ruptures occur. The dashed area in Domain A shows the region that is considered to rupture in tsunami earthquakes. Each slip model is labeled by its event name, year, magnitude, and the domains it is considered to rupture. The color bars indicating amounts of slip are different for each event and featured next to each slip model. Arrows from each slip model to the schematic indicate which domains the event is considered to have ruptured. The white dashed lines are depth contours to the slab in 10-km intervals from Hayes et al. (2018).

(<1–2 m) or no tsunamis. This makes tsunami earthquakes challenging to identify as hazardous in the first minutes, since there is a large discrepancy between the earthquake size and the associated hazard.

Rupture of weak rocks by tsunami earthquakes in Domain A is assumed to radiate seismic waves very inefficiently. This has been seen clearly in the far field (Newman & Okal, 1998). The observation can be leveraged to identify the events with teleseismic recordings (Newman et al., 2011) by measuring their uniquely low ratio of radiated high-frequency energy to earthquake magnitude. This methodology requires far-field teleseismic broadband recordings which means it will not discriminate the event as a tsunami earthquake until after inundation has occurred along the near-source coast. For the 2010 Mentawai earthquake, the final approximate magnitude and its identification as a tsunami event was obtained 16.5 minutes after origin, which was more than 9 min after the first observed tsunami inundation times (Hill et al., 2012; Newman et al., 2011). Studies of the Mentawai earthquake have emphasized the need for new methods to detect tsunami earthquakes in real-time from near-field data, to issue proper warning (Lay et al., 2011).

Near-field recordings of shaking are required to confirm that the high-frequency energy radiation deficit during rupture is manifest in the near field as well. Then perhaps this can be leveraged to provide adequate local tsunami warning. To date, there is little evidence of this diminished high-frequency energy in the near field. Eyewitness reports during the Mentawai earthquake (Hill et al., 2012) consistently suggest that the event produced long-duration, but gentle shaking, but no seismic recordings have existed. Here, we will show previously unstudied strong motion recordings (Figure 2) that confirm the depletion of high-frequency shaking during a tsunami earthquake. With our current understanding of the rupture physics of tsunami earthquakes and the concept of low high-frequency energy radiation per event magnitude, we show that it is possible to use near-field data to discriminate the Mentawai event as a tsunami earthquake, and likely other future events as well. This can be accomplished at least by termination of rupture (1–2 min) and prior to tsunami inundation.

2. Data: Geophysical Observations

The 2010 **M**7.8 Mentawai tsunami earthquake is the only one to have been observed with local and regionally distributed strong motion and High-rate Global Navigation Satellite System (HR-GNSS) data (Figure 2). We anchor our analysis around it. Our approach is twofold. First, we compare the strong motion and

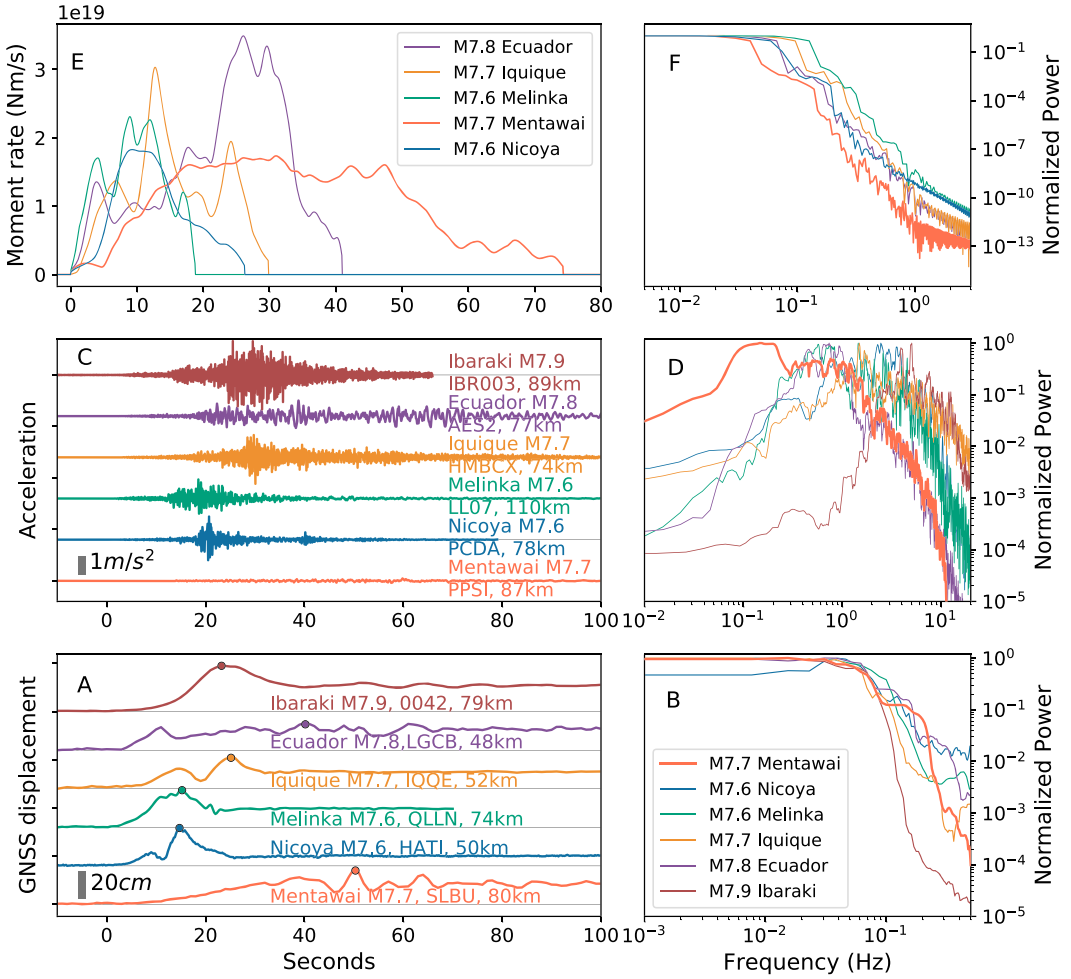

Figure 2. (a) Global Navigation Satellite System displacement waveforms for the east-west component of motion for six earthquakes of similar magnitude. Event name and magnitude, and station names and epicentral distances are indicated in the label below each waveform. The circle indicates the peak ground displacement. (b) Normalized power spectra for the displacement waveforms. (c) Strong motion acceleration waveforms for the north-south component of motion for the same 6 earthquakes as in (a). Event name and magnitude, and station names and epicentral distances are indicated in the label below each waveform. (d) Normalized power spectra for the acceleration waveforms. (e) Source time functions (Vallée & Douet, 2016) for five of the six earthquakes in (a)–(d), these are the same events shown in Figure 1. (f) Normalized source spectra for the source time functions in (e).

HR-GNSS recordings from the Mentawai earthquake to five megathrust events of approximately the same magnitude, which have been well recorded at similar near-field distances (2011 **M**7.9 Ibaraki, Japan; 2012 **M**7.6 Nicoya, Costa Rica; 2014 **M**7.7 Iquique, Chile; 2016 **M**7.6 Melinka, Chile; and 2016 **M**7.8 Pedernales, Ecuador earthquakes). See Text S1in the supporting information for more details. We also analyze the source time functions (STFs, Figure 2) of each of the above megathrust earthquakes that has a similar magnitude to the Mentawai tsunami event. See Text S2 for more details. STFs depict the time evolution of moment release. For this study we have extracted the relevant STFs from the SCARDEC database of Vallée and Douet (2016).

Second, after this detailed analysis, we study a larger dataset of 16 megathrust earthquakes, including the original 5–6 in the same magnitude range as Mentawai, as well as several other megathrust events in the magnitude range **M**7–**M**9 (Table S1). This data set of 16 events includes non-tsunami earthquakes as well as the Mentawai event, so we may establish systematic patterns and propose a real-time discrimination algorithm.

The HR-GNSS data analyzed in this study are from the global database of HR-GNSS recordings from Ruhl et al. (2018), and the strong-motion data are from a follow up global earthquake early warning study by Ruhl et al. (2019). Both of those data sets are freely available, and the peak intensity measures can be found in Table S2. The Mentawai strong motion data are from the Agency for Meteorology, Climatology and Geophysics in Indonesia and made available with this paper as a Zenodo data set (see Acknowledgments).

3. Methods

Strong motion data for a tsunami earthquake have not been previously available. We first study its frequency domain characteristics (Figure 2) by obtaining Fourier power spectra using the multi-taper method (Prieto et al., 2009). We compare the frequency domain behavior of the acceleration data to that of the HR-GNSS data whose spectra is also obtained from multitapers. We also relate the observed behavior to both the time and frequency domain properties of each earthquake's STF.

Additionally, to understand how the behavior of the 2010 Mentawai tsunami earthquake differs from average megathrust earthquakes, we study the ground-motion model (GMM) residuals. GMMs are empirically derived models to predict ground-motion during an earthquake and are typically developed on global datasets of seismic recordings. As such, they represent "mean" earthquake behavior, and GMM residuals show deviations of a particular event's properties from the mean (Baltay & Boatwright, 2015; Sahakian, Baltay, et al., 2018, Sahakian, Melgar, et al., 2018). Using waveforms from the two databases of HR-GNSS and acceleration data (Ruhl et al., 2018, 2019), we find the observed values of peak ground acceleration (PGA), peak ground velocity (PGV), and peak ground displacement (PGD), for near-field sites (<500 km away from the event). PGA and PGV are obtained from the strong motion data while PGD is from the HR-GNSS observations. The ground-motion residual is the observed IM minus the value predicted by a model, in natural logarithm space (Text S4). Positive residuals represent underprediction by the GMM, and negative represent overprediction. We analyze and compare the residuals for these three different intensity measures, as they are each demonstrative of different parts of the earthquake rupture process.

Our underlying hypothesis is that each of these ground motion intensity metrics, PGA, PGV, and PGD, are affected by different parts of the earthquake source process. PGA, as a high-frequency metric, will be representative of the dynamics of the rupture process itself. Meanwhile PGD, as a long-period metric, will reflect mostly the size or magnitude of the earthquake and be far less sensitive to the particularities of the rupture process. So, by looking at the residuals of these metrics simultaneously, it should be possible to recognize anomalous behavior such as that from a tsunami earthquake. We note that unlike PGA and PGV, PGD can only be reliably obtained from HR-GNSS data. Baseline offsets preclude reliable double integration of strong motion data to displacement in real time (Melgar et al., 2015).

The GMMs used to compute PGA, PGV, and PGD residuals are Zhao et al. (2006), Boore et al. (2014), and Melgar et al. (2015), respectively. Some models require knowledge of the site as characterized by the shear wave speed in the top 30 m of the crust (Vs30). We obtain these values for all sites in the data set using the U.S. Geological Survey global terrain-based proxy values (Wald & Allen, 2007; Allen & Wald, 2009; Figure S2). The Vs30 values for the Mentawai sites are all within the range of 290–550 m/s, and as such would cause amplification of PGA (not dampening), if any effect at all.

Kernel density estimate (KDE) plots are calculated using the GMM residuals. Event residuals are obtained by taking the mean of all residuals of one event, representing mean behavior for the earthquake itself.

GMMs also define a model uncertainty, or standard deviation. This represents the average variability expected for a given event magnitude. In addition to observing the PGA residuals themselves, we perform two-sided Kolmogorov-Smirnov (KS) tests to understand if an event's residuals are within the expected variability, given the GMM distribution. The mean of residuals from a GMM distribution is zero, so we take this value and the GMMs standard deviation to represent the model distribution, and we take the mean and standard deviation of an event's residuals to represent its respective distribution. With these KS tests, we also find the magnitude at which the GMM yields a ground-motion distribution demonstrating a p value equal to or larger than the significance level. We call this $\mathbf{M}_{\mathrm{PGA}}$, and it reflects the magnitude of shaking for the earthquake. In addition to this PGA magnitude, we can find a PGD magnitude ($\mathbf{M}_{\mathrm{PGD}}$) using the scaling

laws of Melgar et al., 2015 (described in Text S3). We compare $\mathbf{M}_{PGA}$ to $\mathbf{M}_{PGD}$ by computing $\mathbf{M}_{PGA} - \mathbf{M}_{PGD}$, and can show the inherent difference between high- and low-frequency radiated energy. A strongly negative value of $\mathbf{M}_{PGA} - \mathbf{M}_{PGD}$ indicates that the event is depleted in high-frequency energy.

4. Results and Discussion

4.1. Ground motions

From inspection of the acceleration waveforms at approximately the same hypocentral distance, it is immediately clear that the 2010 Mentawai tsunami earthquake exhibits anomalously low shaking for its magnitude (Figures 2 and S1). The waveform can barely be seen when plotted at the same scale as the other events. Additionally, the normalized spectra for the waveforms clearly show a much lower corner frequency for the Mentawai earthquake than any of the other events, indicating depletion of high-frequency content. This is consistent with the hypothesis that because tsunami earthquakes rupture mostly Domain A, they radiate elastic waves inefficiently. To quantitatively describe the depletion in high-frequency content, we compare intensity measures residuals from a GMM to their expected values from a GMM given the earthquake's magnitude.

To do so we need a reliable rapid estimator of the event's magnitude. Earthquake magnitude for large events at local to regional distances is difficult to estimate in real-time with seismic data alone. HR-GNSS recordings which directly measure crustal deformation are better suited for this task. PGD has been identified as a robust indicator of magnitude even for tsunami earthquakes (Crowell et al., 2016; Melgar et al., 2015). Figure 2 shows why this is the case. The PGD values from HR-GNSS recordings of the Mentawai earthquake are of similar amplitude for comparably sized earthquakes irrespective of what megathrust domains they rupture (Figure 1). This similarity in amplitude is strong evidence that PGD from HR-GNSS closely reflects earthquake moment, unlike strong-motion data, which is strongly affected by the source process. Scaling laws have been derived from PGD observations, and made operational in real time. These relate the observed PGD, as a function of source to site distance, to the final magnitude of an earthquake (Text S4; Melgar et al., 2015; Crowell et al., 2016; Ruhl et al., 2018). Specifically, we applied the algorithm described by Melgar et al. (2015) which inverts the PGD observations and solves for magnitude. We did this in simulated real-time with the HR-GNSS recordings of the Mentawai earthquake, and all other events in the 16-event data set. The $\mathbf{M}_{PGD}$ magnitude values are in Table S1, in all cases $\mathbf{M}_{PGD}$ is obtained within 2 min of earthquake origin time and within 0.1–0.2 magnitude units of the catalog magnitude from the Global CMT Project (globalcmt.org).

The PGA, PGV, and PGD for all strong-motion (PGA and PGV) and GNSS recordings (PGD) of these earthquakes are in Figure 3, along with values from a global database of 16 large (**M**6–**M**9) megathrust earthquakes recorded by both geodetic and strong motion networks (Ruhl et al., 2018; Ruhl et al., 2019). These are plotted along with the estimated values for each intensity measure from ground-motion models (GMMs). It is clear from Figure 3 that the PGA residuals for the Mentawai event are significantly lower than any other event in the database. In fact, a two-sided KS test shows that the null hypothesis (that the Mentawai PGA residuals belong to the same probability density function as the GMM estimated residuals), can be rejected (Figures S3 and S4). Furthermore, these tests show that in order for the Mentawai PGA residuals to belong to the same distribution predicted by the GMM, the magnitude of the Mentawai event would have to be ~**M**6.3. In other words, $\mathbf{M}_{PGA}$ is 6.3 for this event. The ground motions for this tsunami earthquake resemble those of an event nearly 1.5 moment magnitude units smaller than that predicted by the PGD to moment relationships ($\mathbf{M}_{PGA} - \mathbf{M}_{PGD}$ ~−1.5). This is a strong indication that the Mentawai PGA values are much different than those expected from more frequently occurring megathrust events, and this anomalous behavior is distinguishable within several minutes of origin time.

4.2. Implications for Source Processes

Figure 4 shows the PGA, PGV, and PGD event residuals (the mean of all PGA, PGV, or PGD residuals for each event) for each of the 16 events. This indicates average behavior exhibited by the event for a given intensity measure. Unsurprisingly, the PGD residuals for the Mentawai earthquake are similar to those of the other events. This is why the PGD magnitude algorithm is reliable irrespective of the domain being ruptured. In contrast, the PGA event residual for the Mentawai earthquake is very low (Figure 3d).

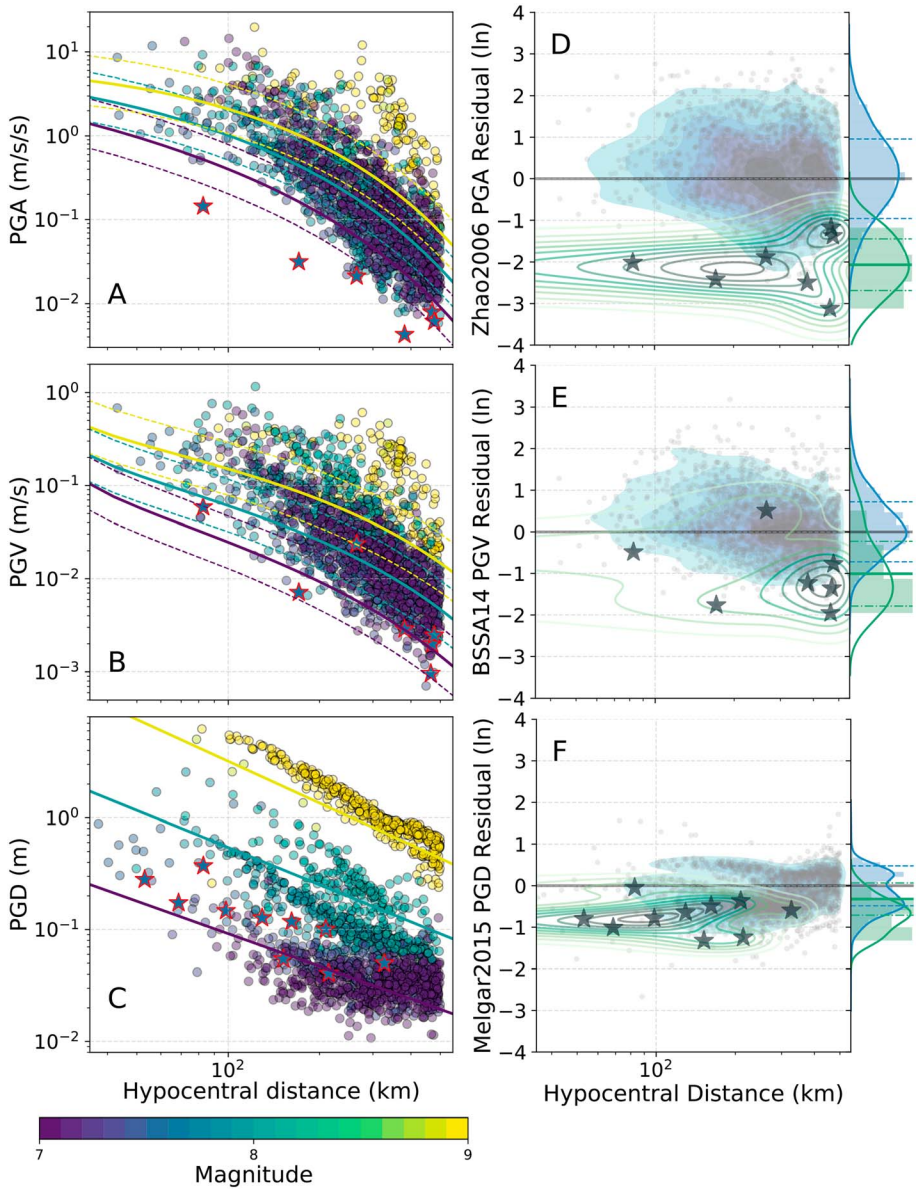

Figure 3. (a) PGA recordings for the 16 earthquakes in this study, scattered and colored by their events' magnitude. Mentawai recordings plotted as stars with a red outline. GMM estimations for PGA are plotted as lines for **M**7, 8, and 9 and colored with the same scheme as the scattered data points. The median ground-motion estimation is plotted as a solid line, and plus or minus one standard deviation as dashed lines. (b) Same as (a), for PGV. (c) Same as (a), for PGD. (d) PGA residual distributions for all 16 events except Mentawai are scattered, and KDE contoured in blue. The residual distribution and histogram are shown on the side *y* axes in blue. The residuals and KDE contour plot for the corresponding Mentawai residuals are shown in green, and the Mentawai residuals plotted as green stars. The Mentawai residual distribution and histograms are shown on the side *y* axes in green. (e) Same as (d) for PGV. (f) Same as (d) for PGD. PGA = peak ground acceleration; PGD = peak ground displacement; PGV = peak ground velocity; KDE = kernel density estimate.

Thus, a consistent view of the rupture process during a tsunami earthquake and its relation to the near-field geophysical observables emerges. The low rigidity and shear wave velocity material that tsunami earthquakes rupture is the main control on the rupture physics of such events. Consider the STFs of the events that have similar magnitudes to the Mentawai earthquake (Figure 2e). The protracted duration of the tsunami earthquake and slow growth to final PGD (Figure 2a; Goldberg et al., 2018), produced by the slow rupture of low rigidity rocks, leads to a low-stress drop rupture (Ye et al., 2016; Yue et al., 2014) with a source

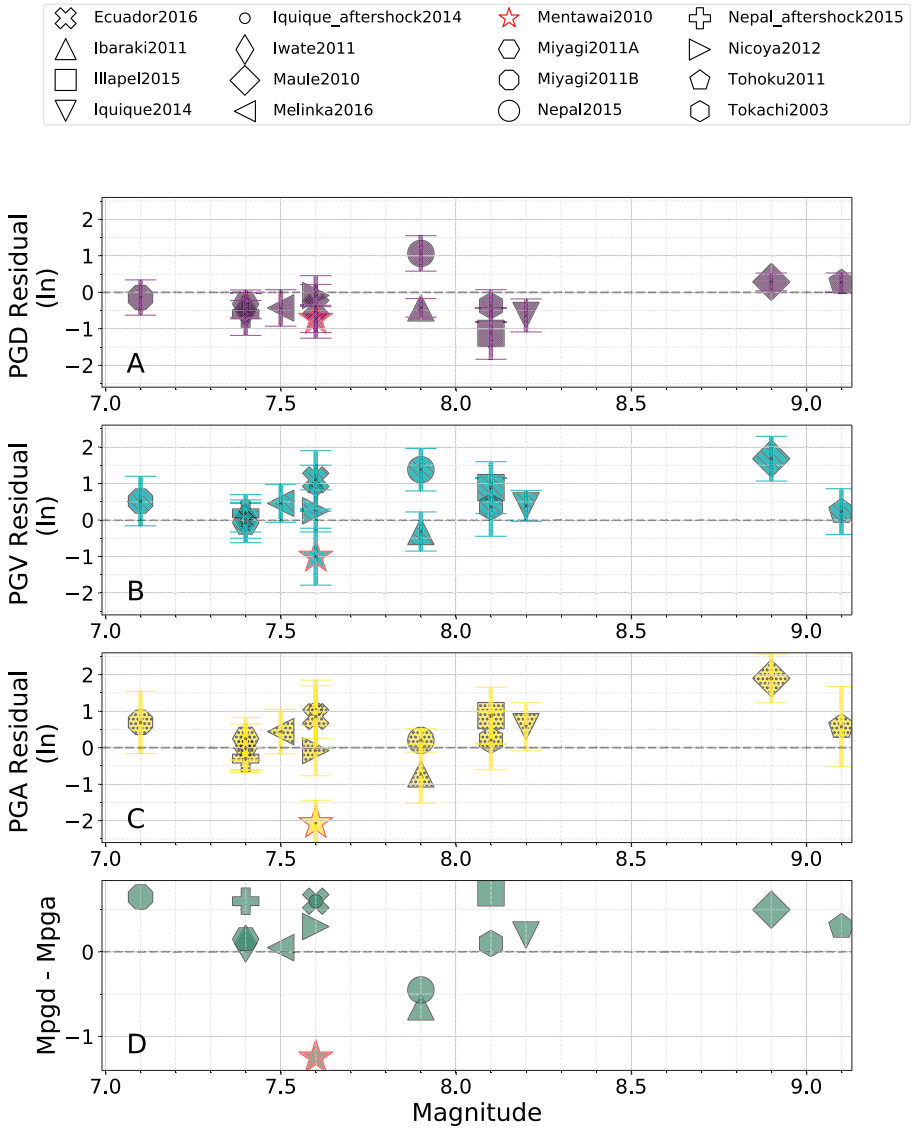

Figure 4. (a) Event residuals for PGD (purple back hashed), (b) PGV (green forward hashed), and (c) PGA (yellow dotted) plotted versus the event's magnitude. The top legend describes each event's symbol. Event residuals are in natural logarithm space, and represent the mean of all residuals (observed − predicted) for each event. Standard deviations on each event's intensity measure are plotted with error bars. (d) $\mathbf{M}_{\mathrm{PGA}} - \mathbf{M}_{\mathrm{PGD}}$ values plotted for each event versus their magnitude. $\mathbf{M}_{\mathrm{PGA}}$ is obtained from the Kolmogorov-Smirnov test results. PGA = peak ground acceleration; PGD = peak ground displacement; PGV = peak ground velocity.

spectrum (Figure 2f) that has a much lower corner frequency for tsunami earthquakes. It also leads to a larger coseismic slip for the given earthquake magnitude, as slip is inversely proportional to rigidity with respect to seismic moment. The net effect is that the distinction between tsunami and traditional megathrust earthquakes will be most conspicuous from the depletion of high frequencies, which can be measured by near-source ground accelerations, herein described with $\mathbf{M}_{\mathrm{PGA}}$. Meanwhile long-period content, described by $\mathbf{M}_{\mathrm{PGD}}$, is mostly unchanged. Diverse near-field geophysical instrumentation can be used to probe these features of the source process. Ground displacements as observed by HR-GNSS inherently reflect the long-period components of ground motion. Comparatively, PGA is most strongly determined from the high-frequency portion of the source spectrum. Indeed, this is what we observe, PGD values (Figure 3) and residuals (Figure 4) unaffected by the high-frequency spectral deficit of the source and PGA values strongly controlled by it. This stark difference both accurately depicts our

understanding of the physics of rupture of tsunami earthquakes, as well as gives us the ability to discriminate between tsunami earthquakes and common megathrust earthquakes (Domains B and C) as soon as the rupture has terminated.

4.3. Toward Real-Time Discrimination

These findings point clearly toward an algorithm that combines HR-GNSS and strong motion observations to identify tsunami earthquakes. It is as follows: First, once the rupture has terminated, acquire the event's magnitude using PGD scaling relationships and the observed PGD from near-field HR-GNSS recordings. Next, compute PGA from near-field strong-motion recordings, and using a suitable GMM, obtain the PGA residuals per recording, as well as an event PGA and PGV residual, for a variety of magnitudes above and below the PGD magnitude of the event. Finally, find the magnitude that best represents the high-frequency shaking ($\mathbf{M}_{\mathrm{PGA}}$), and compare this to $\mathbf{M}_{\mathrm{PGD}}$. A very low residual for PGA or low $\mathbf{M}_{\mathrm{PGA}}$, perhaps coupled with the known hypocentral location, is highly suggestive that the event is rupturing soft, compliant rock near the shallow megathrust and seafloor, yielding a very high likelihood of producing a large tsunami. While we only have good near-field records for one tsunami earthquake it is widely accepted that the conceptual model of the depth-varying properties of megathrusts (Lay et al., 2012) is consistent with previous tsunami earthquakes and with far-field observations (Newman et al., 2011). Furthermore, the high-frequency deficit has been identified in small near-trench earthquakes as well (Singh et al., 2016). Finally, this source information can be used as the initial condition for hydrodynamic models. These can then provide not only information about the earthquake but also rapid forecasts of the expected tsunami amplitudes along the near-source coast (e.g., Hoechner et al., 2013; Melgar et al., 2016). So, while we only have complete near field observations of one tsunami earthquake, in aggregate, our findings strongly argue that by combining diverse observations near-field warning is possible. Public outreach and "natural warning" for tsunami hazards often utilizes the phrase "long or strong, get gone" to communicate to coastal populations that large tsunamis may be imminent following long-duration or strong shaking, an important part of risk awareness and preparedness (Blake et al., 2018; Woods et al., 2017). The implication here is that the long duration might reflect a large magnitude event originating at some distance from the person. During tsunami earthquakes the long source process leads to long-duration shaking as well, however, the recordings from the Mentawai earthquake shown here (Figures 2–4) indicate intensities that are strikingly low. So much so that the population might easily consider themselves safe from harm. Eyewitness accounts of the Mentawai earthquake indicate that the slow and gentle shaking, which lasted for several minutes, was not deemed overly hazardous by many and often it was not felt at all (Hill et al., 2012). Therein lies the challenge and peril of tsunami earthquakes. Near-field geophysical observables, seismic, and geodetic, are now commonplace throughout the world. The results we have presented here are a compelling case that by leveraging and jointly analyzing these diverse datasets, it is possible to discriminate these hazardous events in 1–2 min and to issue warning to populations in the near-source who are most at risk.

5. Conclusions

We studied near-field acceleration, velocity, and displacement data from seismic and geodetic sensors in the near field (<500 km) of 16 megathrust earthquakes. This included the 2010 **M**7.8 Mentawai earthquake, a devastating tsunami earthquake that produced a tsunami runup >16 m in some location. Using these geophysical data, we find that the peak accelerations for the Mentawai earthquake are on par with a **M**6.3 event, yet the displacements are more similar to that expected for the event's magnitude. This suggests that the accelerations are acting as a proxy for radiated energy and the displacements act as a proxy for moment. Thus, these data can be used in real-time to discriminate events as a possible tsunami earthquake, to issue local warning.

Acknowledgments
We are grateful to Christine Ruhl and Dara Goldberg for discussions and help with the strong motion and GNSS data. We also acknowledge the help of colleagues who provided slip models, Han Yue, Jorge Jara, and Jean-Mathieu Nocquet. We also thank Martin Vallée for making his library of source time functions available. We acknowledge the many national agencies who have collected and made available geophysical data. In particular, for the strong motion data of the Mentawai earthquake we would like to thank Agency for Meteorology, Climatology and Geophysics of Indonesia (BMKG). GNSS data are available for download from Ruhl et al. (2018), https://zenodo.org/record/1434374), and strong-motion data are available for download from the Ruhl et al. (2019) paper (https://zenodo.org/record/1469833). Mentawai strong-motion records are available at Zenodo (Sahakian et al., 2019). We thank the GRL Editor and two anonymous reviewers for their time and constructive comments on this paper.

References

Allen, T. I., & Wald, D. J. (2009). On the use of high-resolution topographic data as a proxy for seismic site conditions (Vs30). *Bulletin of the Seismological Society of America*, *99*(2A), 935–943. https://doi.org/10.1785/0120080255

Ammon, C. J., Kanamori, H., Lay, T., & Velasco, A. A. (2006). The 17 July 2006 Java tsunami earthquake. *Geophysical Research Letters*, *33*, L24308. https://doi.org/10.1029/2006GL028005

Baltay, A. S., & Boatwright, J. (2015). Ground-motion observations of the 2014 South Napa earthquake. *Seismological Research Letters*, *86*(2A), 355–360. https://doi.org/10.1785/0220140232

Baptista, A. M., Priest, G. R., & Murty, T. S. (1993). Field survey of the 1992 Nicaragua tsunami. *Marine Geodesy*, *16*(2), 169–203. https://doi.org/10.1080/15210609309379687

Bilek, S. L., & Lay, T. (1999). Rigidity variations with depth along interplate megathrust faults in subduction zones. *Nature*, *400*(6743), 443–446. https://doi.org/10.1038/22739

Blake, D., Johnston, D., Leonard, G., McLaren, L., & Becker, J. (2018). A citizen science initiative to understand community response to the Kaikōura earthquake and tsunami warning in Petone and Eastbourne, Wellington, Aotearoa/New Zealand. *Bulletin of the Seismological Society of America*, *108*(3B), 1807–1817. https://doi.org/10.1785/0120170292

Boore, D. M., Stewart, J. P., Seyhan, E., & Atkinson, G. M. (2014). NGA-West2 equations for predicting PGA, PGV, and 5% damped PSA for shallow crustal earthquakes. *Earthquake Spectra*, *30*(3), 1057–1085. https://doi.org/10.1193/070113EQS184M

Crowell, B. W., Schmidt, D. A., Bodin, P., Vidale, J. E., Gomberg, J., Renate Hartog, J., et al. (2016). Demonstration of the Cascadia G-FAST geodetic earthquake early warning system for the Nisqually, Washington, earthquake. *Seismological Research Letters*, *87*(4), 930–943. https://doi.org/10.1785/0220150255

Faulkner, D. R., Mitchell, T. M., Behnsen, J., Hirose, T., & Shimamoto, T. (2011). Stuck in the mud? Earthquake nucleation and propagation through accretionary forearcs. *Geophysical Research Letters*, *38*, L18303. https://doi.org/10.1029/2011GL048552

Fritz, H. M., Kongko, W., Moore, A., McAdoo, B., Goff, J., Harbitz, C., et al. (2007). Extreme runup from the 17 July 2006 Java tsunami. *Geophysical Research Letters*, *34*, L12602. https://doi.org/10.1029/2007GL029404

Goldberg, D. E., Melgar, D., Bock, Y., & Allen, R. M. (2018). Geodetic observations of weak determinism in rupture evolution of large earthquakes. *Journal of Geophysical Research: Solid Earth*, *123*, 9950–9962. https://doi.org/10.1029/2018JB015962

Hayes, G. P., Moore, G. L., Portner, D. E., Hearne, M., Flamme, H., Furtney, M., & Smoczyk, G. M. (2018). Slab2, a comprehensive subduction zone geometry model. *Science*, *362*(6410), 58–61. https://doi.org/10.1126/science.aat4723

Hill, E. M., Borrero, J. C., Huang, Z., Qiu, Q., Banerjee, P., Natawidjaja, D. H., et al. (2012). The 2010 Mw 7.8 Mentawai earthquake: Very shallow source of a rare tsunami earthquake determined from tsunami field survey and near-field GPS data. *Journal of Geophysical Research*, *117*, B06402. https://doi.org/10.1029/2012JB009159

Hoechner, A., Ge, M., Babeyko, A. Y., & Sobolev, S. V. (2013). Instant tsunami early warning based on real-time GPS–Tohoku 2011 case study. *Natural Hazards and Earth System Sciences*, *13*(5), 1285–1292. https://doi.org/10.5194/nhess-13-1285-2013

Jara, J., Sánchez-Reyes, H., Socquet, A., Cotton, F., Virieux, J., Maksymowicz, A., et al. (2018). Kinematic study of Iquique 2014 Mw 8.1 earthquake: Understanding the segmentation of the seismogenic zone. *Earth and Planetary Science Letters*, *503*, 131–143. https://doi.org/10.1016/j.epsl.2018.09.025

Lay, T., Ammon, C. J., Kanamori, H., Yamazaki, Y., Cheung, K. F., & Hutko, A. R. (2011). The 25 October 2010 Mentawai tsunami earthquake (Mw 7.8) and the tsunami hazard presented by shallow megathrust ruptures. *Geophysical Research Letters*, *38*, L06302. https://doi.org/10.1029/2010GL046552

Lay, T., Kanamori, H., Ammon, C. J., Koper, K. D., Hutko, A. R., Ye, L., et al. (2012). Depth-varying rupture properties of subduction zone megathrust faults. *Journal of Geophysical Research*, *117*, B04311. https://doi.org/10.1029/2011JB009133

Melgar, D., Allen, R. M., Riquelme, S., Geng, J., Bravo, F., Baez, J. C., et al. (2016). Local tsunami warnings: Perspectives from recent large events. *Geophysical Research Letters*, *43*, 1109–1117. https://doi.org/10.1002/2015GL067100

Melgar, D., Crowell, B. W., Geng, J., Allen, R. M., Bock, Y., Riquelme, S., et al. (2015). Earthquake magnitude calculation without saturation from the scaling of peak ground displacement. *Geophysical Research Letters*, *42*, 5197–5205. https://doi.org/10.1002/2015GL064278

Melgar, D., Riquelme, S., Xu, X., Baez, J. C., Geng, J., & Moreno, M. (2017). The first since 1960: A large event in the Valdivia segment of the Chilean Subduction Zone, the 2016 M7. 6 Melinka earthquake. *Earth and Planetary Science Letters*, *474*, 68–75. https://doi.org/10.1016/j.epsl.2017.06.026

Newman, A. V., Hayes, G., Wei, Y., & Convers, J. (2011). The 25 October 2010 Mentawai tsunami earthquake, from real-time discriminants, finite-fault rupture, and tsunami excitation. *Geophysical Research Letters*, *38*, L05302. https://doi.org/10.1029/2010GL046498

Newman, A. V., & Okal, E. A. (1998). Teleseismic estimates of radiated seismic energy: The E/M0 discriminant for tsunami earthquakes. *Journal of Geophysical Research*, *103*(B11), 26,885–26,898. https://doi.org/10.1029/98JB02236

Nocquet, J. M., Jarrin, P., Vallée, M., Mothes, P. A., Grandin, R., Rolandone, F., et al. (2017). Supercycle at the Ecuadorian subduction zone revealed after the 2016 Pedernales earthquake. *Nature Geoscience*, *10*(2), 145–149. https://doi.org/10.1038/ngeo2864

Prieto, G. A., Parker, R. L., & Vernon, F. L. III (2009). A Fortran 90 library for multitaper spectrum analysis. *Computers & Geosciences*, *35*(8), 1701–1710. https://doi.org/10.1016/j.cageo.2008.06.007

Ruhl, C. J., Melgar, D., Chung, A. I., Grapenthin, R., & Allen, R. M. (2019). Quantifying the value of real-time geodetic constraints for earthquake early warning using a global seismic and geodetic dataset. *Journal of Geophysical Research: Solid Earth*, *124*, 3819–3837. https://doi.org/10.1029/2018JB016935

Ruhl, C. J., Melgar, D., Geng, J., Goldberg, D. E., Crowell, B. W., Allen, R. M., et al. (2018). A global database of strong-motion displacement GNSS recordings and an example application to PGD scaling. *Seismological Research Letters*, *90*(1), 271–279.

Sahakian, V., Baltay, A., Hanks, T., Buehler, J., Vernon, F., Kilb, D., & Abrahamson, N. (2018). Decomposing leftovers: Event, path, and site residuals for a small-magnitude Anza region GME. *Bulletin of the Seismological Society of America*, *108*(5A), 2478–2492. https://doi.org/10.1785/0120170376

Sahakian, V. J., Melgar, D., Quintanar, L., Ramírez-Guzmán, L., Pérez-Campos, X., & Baltay, A. (2018). Ground Motions from the 7 and 19 September 2017 Tehuantepec and Puebla-Morelos, Mexico, Earthquakes. *Bulletin of the Seismological Society of America*, *108*(6), 3300–3312.

Sahakian, V. J., Melgar Moctezuma, D., & Muzli, M. (2019). Waveforms from Mentawai 2010 Event Strong-Motion Stations [Data set]. *Geophysical Research Letters*. Zenodo. http://doi.org/10.5281/zenodo.3351683

Singh, S. K., Arroyo, D., Pérez-Campos, X., Rodríguez, Q., Iglesias, A., & Ortiz, M. (2016). Fast Identification of near-trench earthquakes along the Mexican subduction zone based on characteristics of ground motion in Mexico City. *Bulletin of the Seismological Society*, *106*(5), 2071–2080. https://doi.org/10.1785/0120160003

Synolakis, C., Imamura, F., Tsuji, Y., Matsutomi, H., Tinti, S., Cook, B., et al. (1995). Damage, conditions of East Java tsunami of 1994 analyzed. *Eos, Transactions American Geophysical Union*, *76*(26), 257–257. https://doi.org/10.1029/95EO00150

Vallée, M., & Douet, V. (2016). A new database of source time functions (STFs) extracted from the SCARDEC method. *Physics of the Earth and Planetary Interiors*, *257*, 149–157. https://doi.org/10.1016/j.pepi.2016.05.012

Wald, D. J., & Allen, T. I. (2007). Topographic slope as a proxy for seismic site conditions and amplification. *Bulletin of the Seismological Society of America*, *97*(5), 1379–1395. https://doi.org/10.1785/0120060267

Woods, R. J., McBride, S. K., Wotherspoon, L. M., Beavan, S., Potter, S. H., Johnston, D. M., et al. (2017). Science to emergency management response: Kaikoura earthquakes 2016. *Bulletin of the New Zealand Society for Earthquake Engineering*, *50*(2), 329–337. https://doi.org/10.5459/bnzsee.50.2.329-337

Ye, L., Lay, T., Kanamori, H., & Rivera, L. (2016). Rupture characteristics of major and great (Mw≥ 7.0) megathrust earthquakes from 1990 to 2015: 1. Source parameter scaling relationships. *Journal of Geophysical Research: Solid Earth*, *121*, 826–844. https://doi.org/10.1002/2015JB012426

Yue, H., Lay, T., Rivera, L., Bai, Y., Yamazaki, Y., Cheung, K. F., et al. (2014). Rupture process of the 2010 Mw 7.8 Mentawai tsunami earthquake from joint inversion of near-field hr-GPS and teleseismic body wave recordings constrained by tsunami observations. *Journal of Geophysical Research: Solid Earth*, *119*, 5574–5593. https://doi.org/10.1002/2014JB011082

Yue, H., Lay, T., Schwartz, S. Y., Rivera, L., Protti, M., Dixon, T. H., et al. (2013). The 5 September 2012 Nicoya, Costa Rica Mw 7.6 earthquake rupture process from joint inversion of high-rate GPS, strong-motion, and teleseismic P wave data and its relationship to adjacent plate boundary interface properties. *Journal of Geophysical Research: Solid Earth*, *118*, 5453–5466. https://doi.org/10.1002/jgrb.50379

Zhao, J. X., Zhang, J., Asano, A., Ohno, Y., Oouchi, T., Takahashi, T., et al. (2006). Attenuation relations of strong ground motion in Japan using site classification based on predominant period. *Bulletin of the Seismological Society of America*, *96*(3), 898–913. https://doi.org/10.1785/0120050122